Applied Catalysis B: Environmental 243 (2019) 229–235

Contents lists available at ScienceDirect

Applied Catalysis B: Environmental

journal homepage: www.elsevier.com/locate/apcatb

CdS nanorods decorated with inexpensive NiCd bimetallic nanoparticles as efficient photocatalysts for visible-light-driven photocatalytic hydrogen evolution

Bo Wang[a], Sha He[a], Lulu Zhang[a], Xueyan Huang[a], Fan Gao[a], Wenhui Feng[b], Ping Liu[a,*]

[a] Research Institute of Photocatalysis, State Key Laboratory of Photocatalysis on Energy and Environment, Fuzhou University, Fuzhou, 350002, PR China
[b] Hunan Provincial Collaborative Innovation Center for Environment and Energy Photocatalysis, Changsha University, Changsha, 410022, PR China

ARTICLE INFO

Keywords:
NiCd bimetallic nanoparticles
CdS nanorods
Non-noble metal
Photocatalytic H_2 evolution
Charge separation

ABSTRACT

In order to obtain the high H_2 evolution activity, an inexpensive and efficient photocatalyst CdS nanorods decorated with NiCd bimetallic nanoparticles has been designed and successfully prepared via an ingenious in situ deposition method. The experiment results indicate that NiCd bimetallic cocatalysts can efficiently inhibit the recombination of the photoinduced electron-hole pairs and promote the interfacial charge transfer, resulting in a significant improvement in photocatalytic H_2 production performance. The NiCd/CdS NRs sample exhibits an excellent photocatalytic H_2 evolution activity under visible light irradiation ($\lambda > 410$ nm), and the corresponding H_2 evolution rate is 11.57 $mmol{\cdot}h^{-1}{\cdot}g^{-1}$, which is about 64.8, 17.2 and 2.3 times as that of pristine CdS NRs, Cd/CdS and Ni/CdS, respectively. This work is expected to provide a new inspiration for rationally designing highly efficient and practical hybrid photocatalyst systems.

1. Introduction

Photocatalytic water splitting is one of the most appealing technologies for converting low density solar energy into high energy density fuel hydrogen to solve both energy crisis and the environmental problems [1–4]. However, the low quantum efficiency of photocatalytic reaction is still far from accommodating the global future energy demand [5–7]. Constructing an efficient and stable photocatalyst system is a major challenge for us to achieve practical application. As a promising visible light photocatalyst for H_2 evolution, Cadmium sulfide (CdS) has attracted extensive attention because of its broad-range light absorption, high-efficiency photoexciton generation, and suitable photoredox potentials [8,9]. Unfortunately, numerous studies have indicated that pristine CdS suffers from ultrafast recombination of photoexcited carriers and serious photocorrosion [10,11], which severely restrict its extensive application. To overcome these problems, various strategies have been developed during the past decades, such as semiconductor combination, surface sensitization, elements doping, metal loading, textural and crystal modification, etc. [12–15]. Among these strategies, metal, especially noble metal (such as Pt, Au, Pd, and Ru) cocatalysts loading is one of the most typical and promising methods to effectively promote charge spatial separation efficiency [16–18]. Previous studies demonstrate that metal cocatalysts not only act as electron trap, but also provide reactive sites for hydrogen production [16,19]. Generally, the Schottky junction formed at the metal-semiconductor interface would effectively inhibit the charge carriers recombination, resulting in the significant enhancement of photocatalytic H_2 evolution performance. Furthermore, metal cocatalysts loading can improve the stability of photocatalysts to some extent [20]. Even so, the efficiency of photocatalytic H_2 evolution reaction is still too low to achieve the practical application. It is still a huge challenge to further improve the photocatalytic H_2 production performance of monometal loaded photocatalysts.

As a promising way to meet this goal, bimetallic nanoparticle cocatalysts are extensively investigated in photocatalysis, for which the amalgamation of two metals is an approach frequently used to prepare novel materials with superior catalytic performance or other new characteristics compared to monometallic nanoparticles. There is usually a positive synergistic effect between the two metals [21]. The electronic, chemical, and optical properties of the bimetallic particles are remarkably different from their monometallic components due to the change in interatomic distance and band structure with the presence of the second metal component [22]. The optical absorption properties and the reactivity of bimetallic particles are thus different from those of either metal in the bimetallic particles. Various bimetallic nanoparticles, such as AuPt, AuPd, PtPd, AuCu, AuAg, and AuNi have

* Corresponding author.
E-mail address: liuping@fzu.edu.cn (P. Liu).

https://doi.org/10.1016/j.apcatb.2018.10.065
Received 31 July 2018; Received in revised form 21 October 2018; Accepted 25 October 2018
Available online 28 October 2018
0926-3373/

been used as high-efficiency cocatalysts to improve the photocatalytic performance of semiconductor [23–28]. Generally, the bimetal/semiconductor composites exhibit much higher photocatalytic performance than their corresponding monometal/semiconductor counterparts. So far, most of relevant studies for bimetal/semiconductor composites prefer noble metals (such as costly and scarce Au, Ag, Pt, and Pd) [29–34]. As a result, the large scale application of them is severely limited. Therefore, developing inexpensive and efficient noble metal free bimetal cocatalysts is of great urgency. In fact, previous individual study demonstrates that non-noble metals can play similar roles as the above noble metals [16,35,36]. For instance, the Cu-Ni bimetallic system shown activity enhancement in many photocatalytic reactions by enhancing carrier separation compared to their monometallic counterparts [37,38]. However, these semiconductor heterostructures generally suffer from a severe lattice stress because of the different crystalline structures between bimetallic nanoparticles and mastercatalysts, exhibiting a restricted improvement for charge carriers separation efficiency [19,39]. Therefore, how to achieve the continuity of crystalline structures in the interface for insuring high-efficiency transport route would be the key of developing efficient photocatalysts.

Herein, we propose a novel NiCd/CdS nanorods heterojunction photocatalyst as model structure to simultaneously achieve the above goals. We try to develop an ingenious two-step in situ deposition method for constructing the CdS nanorods (CdS NRs) decorated with NiCd bimetallic nanoparticles. First, the Cd/CdS NRs composites are fabricated by an in situ chemical deposition method based on a thermal treatment process. Second, metal Ni is further in situ deposited on the above product with alcohol as solvent and electron donor in the process. A perfect interfacial contact is built between NiCd bimetallic nanoparticles and CdS NRs since they possess the same element, cadmium. And a tight link is formed by sharing cadmium atoms. As a result, a high-efficiency interfacial carriers separation is achieved. As expected that the obtained NiCd/CdS NRs nanocomposite exhibits remarkably enhanced hydrogen evolution performance ($11.57\ mmol{\cdot}h^{-1}\ g^{-1}$) under visible light irradiation ($\lambda > 410$ nm) owing to the efficient interior and interfacial carriers separation as well as the enhanced light absorption. The superior H_2 production rate is approximately 64.8, 17.2 and 2.3 times as that of pristine CdS NRs, Cd/CdS and Ni/CdS, respectively. Our current work may provide new insight into the understanding of the synergetic effect between Ni and Cd. Furthermore, this work may offer an optimized model for constructing novel NiCd/CdS photocatalysts with effective interior and surface carriers separation. Meanwhile, the facile in-situ deposition method is expected to open up a new pathway for designing rationally other highly efficient and practical photocatalysts.

2. Experimental

2.1. Materials

Thiourea ($CS(NH_2)_2$, AR), absolute ethanol (CH_3CH_2OH, AR), sodium sulfite (Na_2SO_3, AR), sodium borohydride ($NaBH_4$, 98%), ethylenediamine ($C_2H_8N_2$, AR), *N,N*-dimethylformamide (DMF, AR), nickel chloride hexahydrate ($NiCl_2{\cdot}6H_2O$, AR), and sodium sulfate (Na_2SO_4, AR) were purchased from Sinopharm Chemical Reagent Co. Ltd. (Shanghai, China). Cadmium nitrate tetrahydrate ($Cd(NO_3)_2{\cdot}4H_2O$, AR) and sodium sulfide nonahydrate ($Na_2S{\cdot}9H_2O$, AR) were obtained from Aladdin Co. Ltd. (Shanghai, China). All chemicals were used directly without further purification. Deionized (DI) water used in the synthesis came from local sources.

2.2. Synthesis of CdS NRs

CdS NRs were prepared via a solvothermal procedure. In a typical run, 5 g $Cd(NO_3)_2{\bullet}4H_2O$ and 3.7 g $CS(NH_2)_2$ were dissolved in 60 mL ethylenediamine under continuous stirring. After about 1 h stirring, the obtained homogenous mixture was transferred into a 100 mL Teflon-lined stainless steel autoclave and heated at 180 ℃ for 24 h. After the autoclave cooled down to room temperature, the resulting precipitates were collected by centrifugation and washed thoroughly with absolute ethanol and deionized water. Then the final products were dried at 60 ℃ overnight in a vacuum oven.

2.3. Synthesis of Cd/CdS NRs composites

The Cd/CdS NRs photocatalyst was in situ synthesized by a modified chemical deposition method [19]. In this synthesis, 200 mg CdS NRs was first placed into a muffle furnace and heated at 400 ℃ for 2 h with a heating rate of 5 ℃/min. After cooling down to room temperature naturally, the obtained powders were dispersed into 50 mL 1 M $NaBH_4$ solution and stirred for about 4 h at room temperature. Then the resulting greenish products were gathered by filtration and rinsed with absolute ethanol and DI water. Finally, the products were dried in vacuum oven at room temperature.

2.4. Synthesis of NiCd/CdS NRs composites

An in situ photoreduction method was carried out to prepare the CdS NRs decorated with NiCd bimetallic nanoparticles. 100 mg as-prepared Cd/CdS NRs composites were dispersed into 30 mL absolute ethanol containing a certain amount of $NiCl_2{\bullet}6H_2O$ under sonication. The suspension was degassed by a vacuum pump and then irradiated by a 300 W xenon lamp ($\lambda > 410$ nm) for 30 min with stirring. The dark green precipitate was filtered and washed with absolute ethanol for several times, and dried at room temperature under vacuum.

2.5. Synthesis of Ni/CdS NRs composites

Ni/CdS NRs sample was synthesized by the same method as NiCd/CdS sample except for replacing Ni/CdS NRs with CdS NRs.

2.6. Characterization

The crystal structures of the as-prepared samples were identified using X-ray diffraction (XRD) patterns carried out on a Bruker D8 ADVANCE X-ray diffractometer via Cu Kα radiation ($l = 0.15418$ nm), which were operated at 40 kV and 40 mA. The scan rate was 0.5 ($2\theta\ s^{-1}$). UV–vis diffuse reflectance spectroscopy (DRS) was recorded on a Carry 500 UV–vis spectrophotometer, during which $BaSO_4$ was served as the reference. Scanning electron microscopy (SEM) images were collected using a field-emission scanning electron microscope (FESEM, HITACHISU8000). Transmission electron microscopy (TEM) and high-resolution transmission electron microscopy (HR-TEM) images were obtained on a Tecnai G2F20 S-TWIN electron microscope with a 200 kV accelerating voltage. X-ray photoelectron spectroscopy (XPS) analysis was conducted on a Thermo Scientific ESCALAB 250 photoelectron spectrometer with a monochromatic Al Kαas the X-ray source and hemispherical analyzer. The binding energies were corrected with reference to the C 1 s peak of the surface adventitious carbon at 284.8 eV. Photoluminescence (PL) emission spectra of samples were obtained using a FLS980 fluorescence spectrometer, which were excited by 400 nm light at room temperature.

2.7. Photocatalytic activity measurements

The photocatalytic performance of the NiCd/CdS NRs composites was investigated by photocatalytic H_2 production reaction under visible light irradiation, which was carried out on a commercial reaction system (LabSolar 6 A, Perfect Light Co.). Typically, 20 mg of the as-prepared sample was dispersed by sonication into 100 mL mixed solution containing Na_2S (0.1 mol/L) and Na_2SO_3 (0.1 mol/L) as sacrificial reagents, and the suspension was poured into a Pyrex top-irradiation

quartz reaction reactor. The vessel was then degassed using a vacuum pump for a fixed time to remove the residual air. The aforementioned 300 W xenon lamp (λ > 410 nm) was used as a visible light source to vertically irradiate the reaction cell to generate hydrogen. The obtained H_2 was measured every 1 h by an online gas chromatograph (GC7900, Techcomp, Shanghai) equipped with a thermal conductivity detector, and Ar as the carrier gas. The solution temperature was controlled at 5 ℃ by a recirculated water cooling system throughout the entire process.

2.8. Photoelectrochemical measurements

The photocurrents of the prepared samples were operated on a CHI660E electrochemical workstation equipped with a standard three-electrode system. The counter and reference electrodes were Pt plate and Ag/AgCl, respectively, and 0.2 M Na_2SO_4 solution (pH = 6.8) was used as the electrolyte. A ZENNIUM electrochemical workstation (Zahner, Germany) was utilized to monitor the electrochemical impedance spectroscopy (EIS) of the products in the mixed solution of 10 mM $K_3Fe(CN)_6/K_4Fe(CN)_6$ and 0.5 M KCl. Linear sweep voltammetry (LSV) was performed in the mixed solution of 0.1 M Na_2S and 0.1 M Na_2SO_3 with a scan rate of 10 mV s^{-1} in the above-mentioned three-electrode cell. 5 mg of the as-prepared sample powder was ultrasonically dispersed into DMF solution (0.5 mL), and then the slurry (20 μL) was evenly spread in a 0.5 × 0.5 cm^2 window on fluorine-doped tin oxide (FTO) glass substrate and dried at room temperature under vacuum. Finally, the uncovered parts of the working electrode were painted with insulating epoxy resin. A xenon lamp (300 W) equipped with a cutoff filter (λ > 410 nm) was used as visible light source.

3. Results and discussion

Scheme 1 illustrates the preparation route of the NiCd/CdS NRs photocatalyst. First, the Cd/CdS NRs composites were synthesized by a previously reported in situ chemical reduction method based on a thermal treatment process [19]. Then, the metal Ni was further deposited on the Cd/CdS NRs via a photoreduction procedure. Photo-induced electrons will directionally transfer to metallic Cd from CdS NRs under visible light irradiation so that Ni metal can be selectively anchored on the metallic Cd, as a consequence, the final NiCd bimetallic nanoparticles decorated CdS NRs photocatalyst is obtained. Besides, for comparision, Ni/CdS NRs sample was prepared by a similar photodeposition process. The details of the synthesis of all samples have been described in the experimental section.

XRD patterns of the as-prepared samples are characterized to investigate their crystallographic structure and phase purity. As displayed in Fig. 1, the diffraction peaks of pristine CdS NRs could be well-matched with the hexagonal wurtzite structure CdS (JCPDS no. 41-1049, a = 4.14 Å and c = 6.72 Å). The deposition of Cd, Ni, or NiCd bimetallic nanoparticles does not change the essential crystallographic structure of CdS NRs. The peaks at 31.84°, 34.75° and 38.37° in the XRD patterns of Cd/CdS NRs sample could be indexed to the (002), (100) and (101) planes of metallic Cd (JCPDS no. 65-3363), respectively, which confirm the formation of metallic Cd on CdS NRs composite. Interestingly, the diffraction peaks of metallic Cd disappear from the NiCd/CdS diffraction pattern after the introduction of metallic Ni,

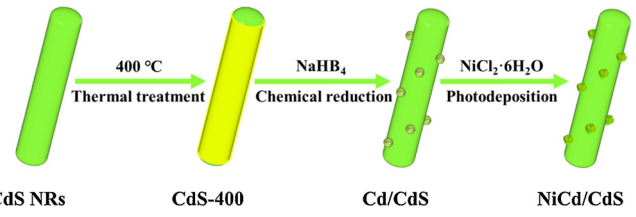

Scheme 1. Schematic preparation process for the NiCd/CdS NRs photocatalysts.

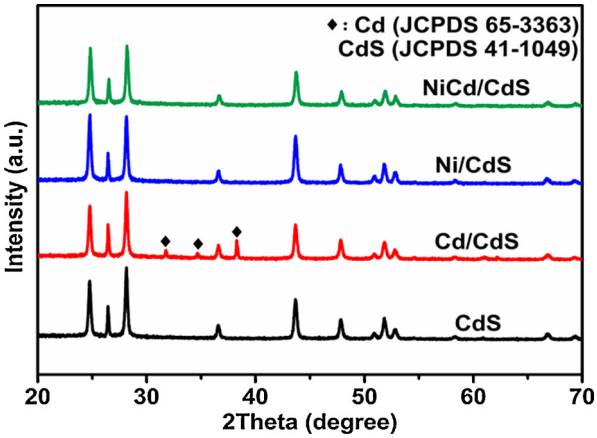

Fig. 1. Typical XRD patterns of the as-prepared photocatalysts.

which may be ascribed to the fact that the second metal component changes the diffraction property of the metal Cd or its crystal structure. More evidences of existing Ni and Cd have been given in other characterizations.

Fig. 2a and Fig. 2b present the SEM images of the as-prepared pure CdS NRs and the NiCd/CdS NRs composite, respectively. As can be seen, CdS NRs has a rod shape with a diameter of 30–80 nm. The morphology of CdS NRs is not affected visibly during the subsequent synthesis procedure. Meanwhile, some particles are found on the surface of NiCd/CdS NRs sample as shown in Fig. 2b. In order to further confirm the morphology and composition of the obtained NiCd/CdS NRs composite, TEM and HRTEM were carried out. It can be seen in Fig. 2c, nanoparticles with size of 10–40 nm have been successfully assembled on the surface of CdS nanorods. The TEM image agrees well with the SEM observation. In addition, the HRTEM image in Fig. 2d (Fig. 2d is a partial enlarged view of the portion shown in the square frame of Fig. 2c) indicates the high crystallinity of the NiCd/CdS NRs photocatalyst, as evidenced by well-defined lattice fringes. The clear lattice fringes with interplanar d-spacing of about 0.34 nm, 0.28 nm and 0.18 nm correspond to the (002) lattice plane of hexagonal CdS, (002) crystal plane of metallic Cd and (200) plane of metallic Ni, respectively [19,40,41]. These results further reveal that NiCd bimetallic nanoparticles are successfully anchored onto the surface of CdS NRs via the aforementioned in situ deposition method.

XPS analysis is performed to further confirm the composition of the NiCd/CdS NRs and explore the interaction between NiCd bimetallic nanoparticles and CdS NRs. As shown in Fig. 3a, Cd 3d spectra of pure CdS NRs are composed of two peaks at about 404.9 and 411.7 eV, which could be respectively ascribed to Cd $3d_{5/2}$ and Cd $3d_{3/2}$ of Cd^{2+} in pristine CdS NRs. Yet for the NiCd/CdS NRs composite, two new peaks can be observed at approximately 404.4 and 411.2 eV, which could be attributed to Cd $3d_{5/2}$ and Cd $3d_{3/2}$ of metallic Cd, respectively. After the in situ deposition of NiCd bimetallic nanoparticles, an obvious shift for about 0.2 eV toward higher binding energy can be noticed in Cd 3d spectra, which indicates a strong interfacial interaction between the loaded NiCd bimetal and CdS NRs [19]. Fig. 3b shows the Ni $2p_{3/2}$ XPS spectra of the as-prepared NiCd/CdS NRs sample. In the resultant spectrum, the peak at 852.0 eV can be assigned to metallic Ni, and peaks at about 856.4, 860.2, and 861.7 eV could be ascribed to Ni^{2+} and NiO, respectively [41–43]. The partial oxidation of the metal Ni may be caused by the exposure of samples to air during the preparation and storage steps. The thin oxide layer is only formed on the surface, and can restrain the further oxidation of the Ni metal [35]. The above results indicate that CdS, Cd, and Ni coexisted in the NiCd/CdS NRs photocatalyst, also reveal a strong interfacial interaction between the loaded bimetallic NiCd and CdS NRs.

The optical performances of as-prepared pristine CdS NRs and

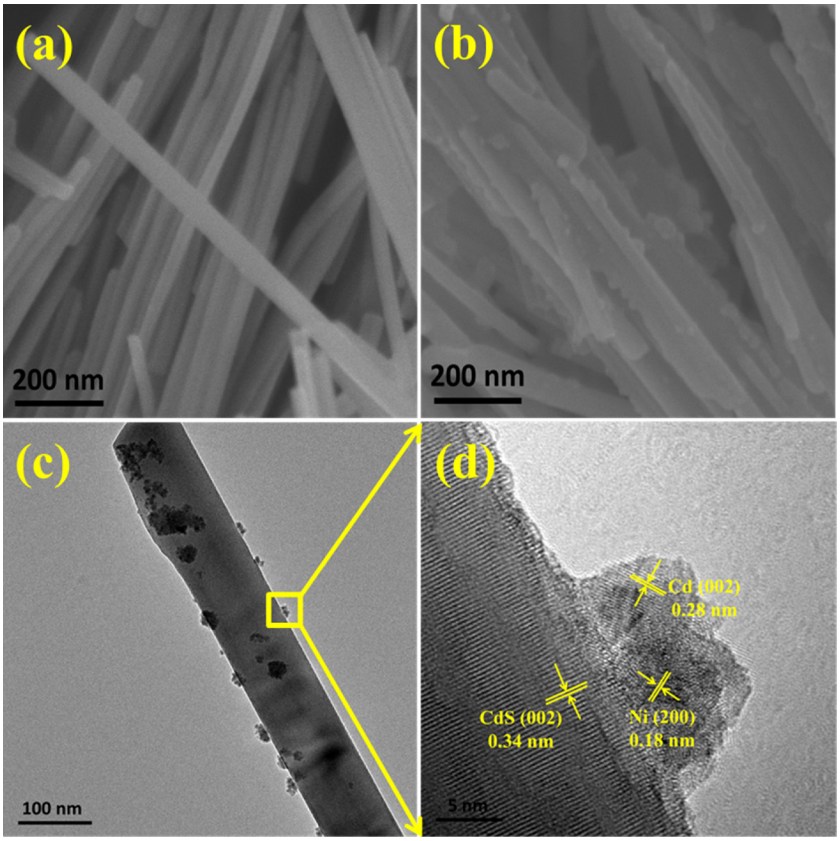

Fig. 2. SEM images of (a) pure CdS NRs and (b) NiCd/CdS NRs composite; (c) TEM and (d) HRTEM images of NiCd/CdS NRs sample.

NiCd/CdS NRs nanocomposite are investigated using UV–vis diffuse reflectance spectroscopy (DRS) [44]. As shown in Fig. 4, all of the samples present a similar absorption edge at about 530 nm, which can be attributed to the essential band gap absorption of CdS. After modified with Cd, Ni or NiCd nanoparticles, a significantly enhanced absorption in the range of 530–800 nm can be observed. By contrast, the NiCd/CdS NRs sample displays the strongest absorption in the visible light area. Such absorption order of the as-prepared samples is in accordance with the color change (as shown in inset of Fig. 4). These results demonstrate that the coupling of NiCd bimetallic nanoparticles could be responsible for the optimized optical property of NiCd/CdS NRs composite. The significantly enhanced light absorption may result in an improved photocatalytic H_2 production performance. Furthermore, the bandgap energy values (Eg) of the samples are estimated by extrapolating the linear plots of the Kubelka-Munk function versus the exciting light energy. As shown in Fig. S1, the E_g of CdS NRs, Cd/CdS NRs, Ni/CdS NRs, and NiCd/CdS NRs are approximately 2.46, 2.44, 2.45, and 2.43 eV, respectively, suggesting that the bandgap of CdS NRs is affected slightly by the modification. In order to reveal how the strong binding between NiCd bimetal and CdS NRs impact the charge carrier dynamics of the composite system, the photoluminescence (PL) emission spectra of the as-prepared samples are collected and depicted in Fig. 5. The PL emission peak at about 530 nm (photoexcited by 400 nm) could be ascribed to the intrinsic excitonic emission of CdS, which is in accordance with its band gap energy of 2.4 eV [45]. The intensity of this PL emission peak is remarkably decreased when loaded with Cd, Ni or NiCd nanoparticles. Notably, the NiCd/CdS NRs sample presents the weakest PL emission peak. It indicates that NiCd bimetal can more effectively suppress the recombination of photoexcited electron-hole pairs than single Cd or Ni metal. The electrochemical impedance spectroscopy (EIS) and transient photocurrent response are performed to investigate the electrical properties of all the as-prepared

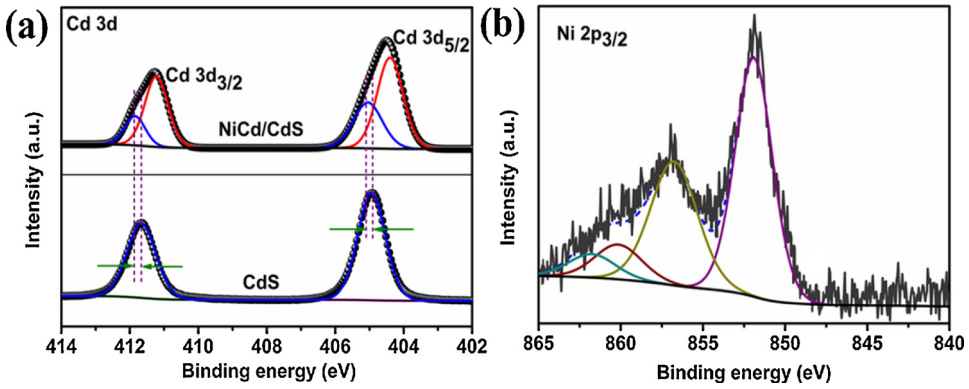

Fig. 3. The high-resolution XPS spectra of (a) Cd 3d of CdS NRs and NiCd/CdS NRs and (b) Ni $2p_{3/2}$ of NiCd/CdS NRs sample.

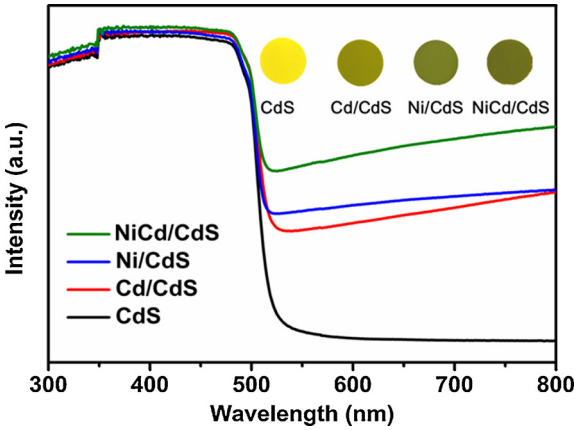

Fig. 4. UV–vis DRS patterns of the as-prepared samples. Insert: the color of CdS NRs, Cd/CdS NRs, Ni/CdS NRs, and NiCd/CdS NRs composites.

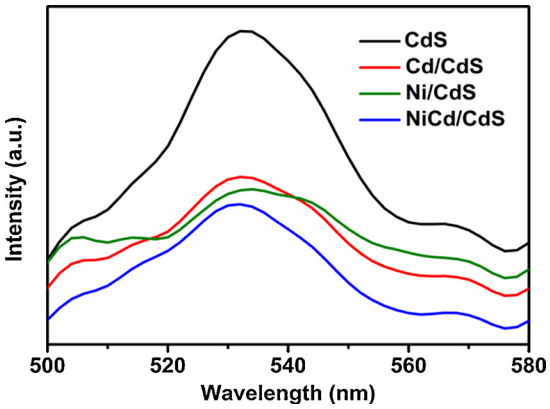

Fig. 5. PL emission spectra of the as-obtained photocatalysts.

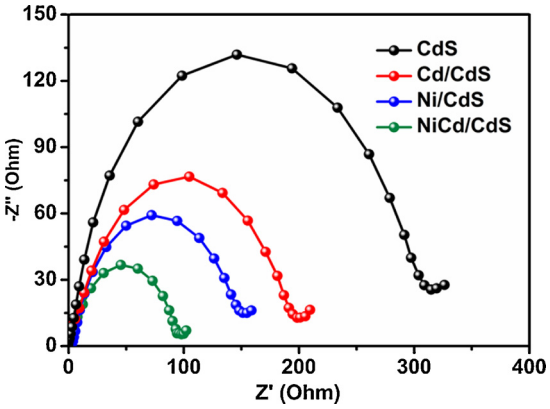

Fig. 6. EIS Nyquist plots of the bare and modified CdS NRs.

samples [46,47]. As can be seen in Fig. 6, the Nyquist arc radius of Cd/CdS NRs and Ni/CdS NRs decreased dramatically compared to that of pristine CdS NRs, while NiCd/CdS NRs exhibited a further decrease. It is suggested a more efficient interfacial charge transfer of NiCd/CdS NRs, which probably attributes to the fact that the NiCd bimetal has stronger electron attraction and more intimate interface contact with CdS nanorods. The in situ deposition of metallic Cd effectively minimizes the lattice stress between mastercatalyst and cocatalyst, resulting in remarkably reduced impedance for the photoinduced electrons transfer. The metal Ni deposited on the metallic Cd further promotes the ability for attracting electrons. As further evidence, the transient photocurrent response recorded for several light on-off cycles is detected under

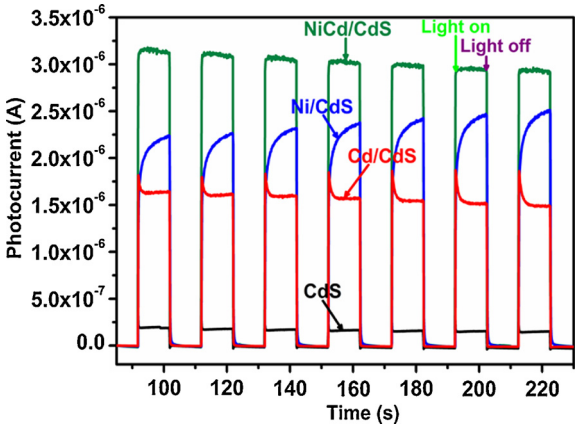

Fig. 7. Transient photocurrent response of CdS NRs, Cd/CdS NRs, Ni/CdS NRs, and NiCd/CdS NRs photocatalysts.

visible light irradiation (λ > 410 nm) and displayed in Fig. 7. It can be clearly seen that the NiCd/CdS NRs photocatalytic system presents the highest photocurrent density among the as-prepared samples, indicating that NiCd bimetallic nanoparticles modified CdS NRs possess much higher charge transfer efficiency than that of Cd/CdS NRs and Ni/CdS NRs monometallic composite [48–51]. These results further confirm that the in situ deposited NiCd bimetal can effectively inhibit the recombination of the photoinduced electron-hole pairs and make more electrons flow out to participate in the reactions. This also means the possibility of higher photocatalytic activity for the NiCd/CdS NRs sample.

The polarization curves of the samples are recorded to reveal the potential of them for superior performance in hydrogen evolution reactions. As shown in Fig. 8, NiCd/CdS NRs sample displays a much smaller onset potential (-0.85 V *vs.* Ag/AgCl) than Cd/CdS NRs (-1.08 V *vs.* Ag/AgCl) and Ni/CdS NRs (-1.0 V *vs.* Ag/AgCl), demonstrating the advantages of its unique structure (for example, the enhanced electrical conductivity of this system) [52,53]. Yet pure CdS NRs sample exhibits very high onset overpotential, which can be attributed to its large electron transport impedance, as revealed in Fig. 6. Based on the above empirical analysis, the as-obtained NiCd/CdS NRs sample is expected to be a superior photocatalyst. To verify this expectation, the activity of all the as-prepared samples for the photocatalytic water splitting to produce H_2 is performed under visible light irradiation (λ > 410 nm) in an aqueous solution containing Na_2S/Na_2SO_3 as sacrificial agents. The increase of H_2 for all samples shows almost a linear with irradiation time (Fig. 9a). Meanwhile, it can be seen that the bare CdS NRs only shows a limited photocatalytic activity for H_2 evolution, which may be ascribed to the fast recombination of photoinduced electrons and holes, while the CdS NRs in situ loaded by metal exhibit dramatically

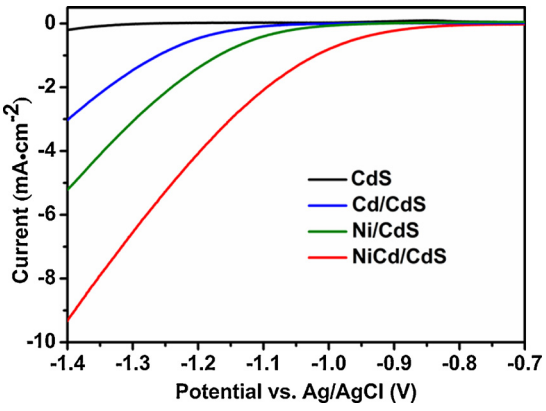

Fig. 8. Polarization curves for all samples.

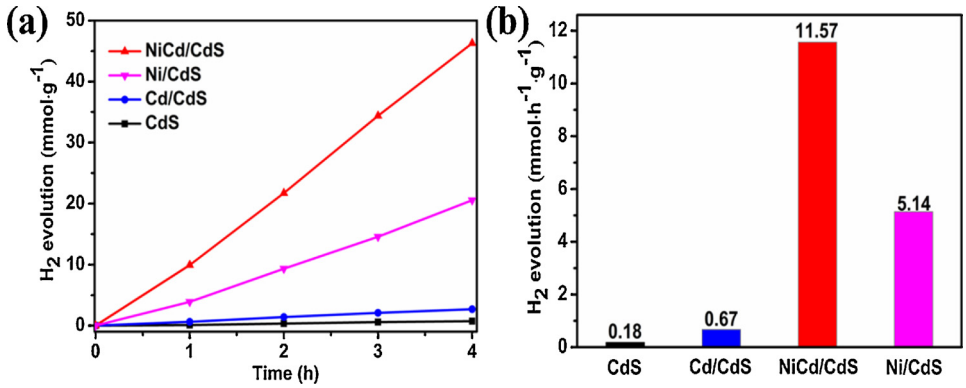

Fig. 9. (a) The time courses of H_2 evolution over the as-prepared photocatalysts. (b) Comparison of H_2 evolution rates of the as-obtained samples under visible light irradiation ($\lambda > 410$ nm).

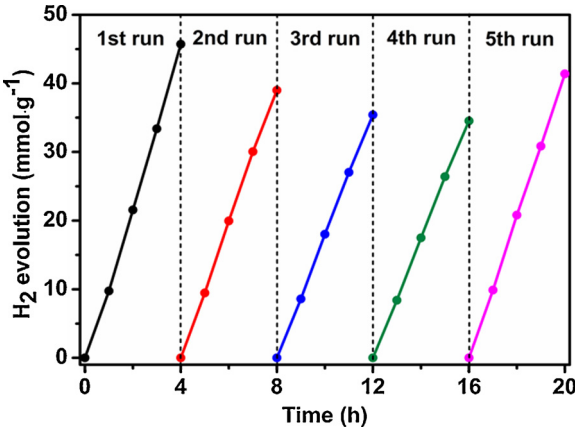

Fig. 10. Cycling test over the NiCd/CdS NRs composite under visible light ($\lambda > 410$ nm).

improved photoactivities and the activities enhance in the order of Cd/CdS < Ni/CdS < NiCd/CdS. The sample co-loaded with Cd and Ni presents the highest photocatalytic H_2 evolution performance. For a more quantitative comparison, the corresponding average photocatalytic H_2 production rates of the samples are calculated and summarized in Fig. 9b. Notably, the NiCd/CdS sample shows the optimal performance and the H_2 evolution rate is as high as 11.57 mmol·h^{-1} g^{-1}, which is about 64.8, 17.2 and 2.3 times higher as that of pure CdS NRs, Cd/CdS and Ni/CdS, respectively. Furthermore, for comparison, Pt/CdS was prepared via a photoreduction process, and photocatalytic H_2 evolution measurement was performed under the same condition. As can be seen in Fig. S2, the H_2 generation rate of NiCd/CdS is almost 3.6 times higher as that of Pt/CdS. These encouraging results suggest an obvious synergetic effect between the Ni and Cd, and the NiCd bimetal deposited by situ has an enormous potential to further improve the performance for photocatalytic H_2 evolution. As we know, the stability of photocatalyst is critical for practical application. Fig. 10 shows the result of cycling experiment executed on photocatalytic H_2 evolution activity. A linear increase of H_2 with irradiation time can be observed in each run and the lines are nearly parallel to each other. A slight decline of H_2 production rate can be found after four consecutive runs without renewing the reagents and photocatalysts, which may be resulted from the consumption of sacrificial agents. To prove this hypothesis, the system was supplemented by a certain amount of Na_2S and Na_2SO_3. As a result, a recovery of H_2 production rate can be observed in the 5th run. Besides, XRD patterns and SEM images of NiCd/CdS NRs photocatalyst before and after five

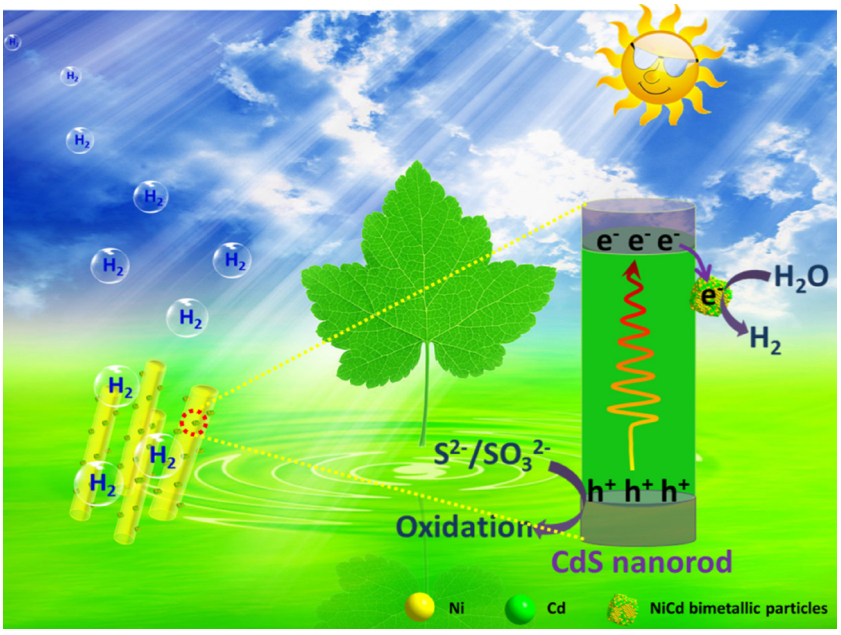

Scheme 2. Illustrative diagrams of a visible-light-driven photocatalytic H_2 evolution mechanism over the constructed NiCd/CdS NRs photocatalyst system.

runs for photocatalytic H_2 production were collected, which are shown in Fig. S3 and Fig. S4, respectively. It is clear that no apparent change for both the crystal structure and morphology of NiCd/CdS NRs composite can be observed after photocatalytic reaction for 20 h. These results verify that the obtained NiCd/CdS NRs sample possesses good stability during the photocatalytic process. Based on the above experimental results and analysis, a probable mechanism for the photocatalytic H_2 evolution process is briefly illustrated in Scheme 2. The in-situ deposition process ensures that NiCd bimetal could be intimately anchored on CdS NRs. Photoexcited electron-hole pairs are generated in CdS NRs illuminated with visible light, the electrons are excited to the conduction band (CB) from the valence band (VB) of CdS, while the holes are left in the VB. When the photoinduced electrons transfer from the CdS NRs bulk to its surface and concentrate in intimate binding site, the electrons rapidly flow through the interface channel to NiCd bimetallic nanoparticles where they reduce H^+ to produce H_2. Meanwhile, the photoexcited holes are consumed by the sacrificial reagents to induce oxidized products. In this photocatalytic system, NiCd bimetallic nanoparticles not only act as excellent electron traps but also can supply abundant hydrogen production sites. Consequently, the CdS NRs in situ decorated with NiCd bimetal achieve superior photocatalytic H_2 evolution activity and good stability. Even so, it should be noted that more evidence is still required to further reveal the structure of NiCd/CdS NRs, as well as the junction between NiCd and CdS NRs.

4. Conclusions

In summary, CdS nanorods decorated with NiCd bimetallic nanoparticles have been successfully fabricated via an ingenious two-step in situ deposition method in this work. The NiCd/CdS NRs system shows a superior photocatalytic H_2 production performance, with a H_2 evolution rate of 11.57 $mmol \cdot h^{-1} g^{-1}$, which is about 64.8, 17.2 and 2.3 times as that of pure CdS NRs, Cd/CdS and Ni/CdS, respectively. This excellent photocatalytic activity could be ascribed to the combined effects of the factors as follows: (1) the enhanced light absorption intensity; (2) more efficient charge separation, and faster interfacial charge migration due to the intimate interfacial contact between bimetallic NiCd and CdS NRs; (3) more abundant surface active sites for the photocatalytic H_2 evolution reaction; (4) a shorter electron diffusion length owing to the 1D nanorods structure. This work may provide new insight into the understanding of the synergetic effect between Ni and Cd. Meanwhile, the facile in-situ deposition method in this work is expected to open up a new avenue for the rational design of other highly efficient and practical photocatalyst systems.

Acknowledgement

This work is supported by the National Natural Science Foundation of China (21473031, 21673041).

Appendix A. Supplementary data

Supplementary material related to this article can be found, in the online version, at doi:https://doi.org/10.1016/j.apcatb.2018.10.065.

References

[1] F.E. Osterloh, Chem. Soc. Rev. 42 (2013) 2294–2320.
[2] K. Maeda, K. Domen, J. Phys. Chem. Lett. 1 (2010) 2655–2661.
[3] X. Zou, Y. Zhang, Chem. Soc. Rev. 44 (2015) 5148–5180.
[4] A.J. Esswein, D.G. Nocera, Chem. Rev. 107 (2007) 4022.
[5] H. Chen, Z. Sun, S. Ye, D. Lu, P. Du, J. Mater. Chem. A 3 (2015) 15729–15737.
[6] X. Li, J. Yu, M. Jaroniec, Chem. Soc. Rev. 45 (2016) 2603–2636.
[7] J. Yang, D. Wang, H. Han, C. Li, Acc. Chem. Res. 46 (2013) 1900–1909.
[8] M. Seol, H. Kim, Y. Tak, K. Yong, Chem. Commun. 46 (2010) 5521–5523.
[9] J. Ran, J. Yu, M. Jaroniec, Green Chem. 13 (2011) 2708–2713.
[10] W. Jiang, Y. Liu, R. Zong, Z. Li, W. Yao, Y. Zhu, J. Mater. Chem. A 3 (2015) 18406–18412.
[11] N. Zhang, S. Liu, X. Fu, Y.J. Xu, J. Mater. Chem. 22 (2012) 5042–5052.
[12] J. Chen, F. Qiu, W. Xu, S. Cao, H. Zhu, Appl. Catal. A Gen. 495 (2015) 131–140.
[13] H. Wang, L. Zhang, Z. Chen, J. Hu, S. Li, Z. Wang, J. Liu, X. Wang, Chem. Soc. Rev. 45 (2015) 5234–5244.
[14] A.B. Djurišić, Y.H. Leung, A.M.C. Ng, Mater. Horiz. 1 (2014) 400–410.
[15] B. Qiu, Q. Zhu, M. Du, L. Fan, M. Xing, J. Zhang, Angew. Chemie 129 (2017) 2728–2732.
[16] H. Li, H. Yu, L. Sun, J. Zhai, X. Han, Nanoscale 7 (2015) 1610–1615.
[17] A. Tanaka, K. Teramura, S. Hosokawa, H. Kominami, T. Tanaka, Chem. Sci. 8 (2017) 2574.
[18] H. Guo, M. Kemell, M. Heikkilä, M. Leskelä, Appl. Catal. B 95 (2010) 358–364.
[19] B. Wang, S. He, W. Feng, L. Zhang, X. Huang, K. Wang, S. Zhang, P. Liu, Appl. Catal. B 236 (2018) 233–239.
[20] W. Choi, G. Park, K.-L. Bae, J.Y. Choi, K.M. Nam, H. Song, J. Mater. Chem. A 4 (2016) 13414–13418.
[21] M. Arenz, V. Stamenkovic, T.J. Schmidt, K. Wandelt, P.N. Ross, N.M. Markovic, J. Chem. Soc. Faraday Trans. 5 (2003) 4242–4251.
[22] J. Ding, X. Li, L. Chen, X. Zhang, X. Tian, Appl. Catal. B 224 (2018) 322–329.
[23] F. Wang, Y. Jiang, D.J. Lawes, G.E. Ball, C. Zhou, Z. Liu, R. Amal, ACS Catal. 5 (2015) 3924–3931.
[24] T.K. Rahul, M. Mohan, N. Sandhyarani, ACS Sustain. Chem. Eng. 6 (2018) 3049–3059.
[25] F. Mushtaq, A. Asani, M. Hoop, X.Z. Chen, D. Ahmed, B.J. Nelson, S. Pané, Adv. Funct. Mater. 26 (2016) 6995–7002.
[26] Ş. Neaţu, J.A. Maciáagulló, P. Concepción, H. Garcia, J. Am. Chem. Soc. 136 (2014) 15969–15976.
[27] N. Zhou, L. Polavarapu, N. Gao, Y. Pan, P. Yuan, Q. Wang, Q.H. Xu, Nanoscale 5 (2013) 4236–4241.
[28] H. Wang, D. Liu, C. Xu, Catal. Sci. Technol. 6 (2016) 7137–7150.
[29] P. Dong, B. Yang, C. Liu, F. Xu, X. Xi, G. Hou, R. Shao, RSC Adv. 7 (2017) 947–956.
[30] Y. Xin, L. Wu, L. Ge, C. Han, Y. Li, S. Fang, J. Mater. Chem. A 3 (2015) 8659–8666.
[31] J. Ding, X. Li, L. Chen, X. Zhang, S. Sun, J. Bao, C. Gao, X. Tian, J. Mater. Chem. A 4 (2016) 12630–12637.
[32] F. Wang, Y. Jiang, X. Wen, J. Xia, G. Sha, R. Amal, Chemcatchem 5 (2013) 3557–3561.
[33] J. Zhang, Y. Lu, L. Ge, C. Han, Y. Li, Y. Gao, S. Li, H. Xu, Appl. Catal. B 204 (2017) 385–393.
[34] T. Jiang, C. Jia, L. Zhang, S. He, Y. Sang, H. Li, Y. Li, X. Xu, H. Liu, Nanoscale 7 (2014) 209–217.
[35] B. Wang, W. Feng, L. Zhang, Y. Zhang, X. Huang, Z. Fang, P. Liu, Appl. Catal. B 206 (2017) 510–519.
[36] S. Zhou, M. Wen, N. Wang, Q. Wu, Q. Wu, L. Cheng, J. Mater. Chem. 22 (2012) 16858–16864.
[37] P. Zhang, T. Song, T. Wang, H. Zeng, J. Mater. Chem. A 5 (2017) 22772–22781.
[38] Z. Lin, J. Li, L. Li, L. Yu, W. Li, G. Yang, J. Mater. Chem. A 5 (2017) 773–781.
[39] W. Feng, Y. Wang, X. Huang, K. Wang, F. Gao, Y. Zhao, B. Wang, L. Zhang, P. Liu, Appl. Catal. B 220 (2018) 324–336.
[40] J. Zhao, C. Ye, X. Fang, Y. Peng, Z. Wang, L. Zhang, J. Cryst. Growth 277 (2005) 445–449.
[41] Z. Chai, T.-T. Zeng, Q. Li, L.-Q. Lu, W.-J. Xiao, D. Xu, J. Am. Chem. Soc. 138 (2016) 10128–10131.
[42] T. Simon, N. Bouchonville, M.J. Berr, A. Vaneski, A. Adrovic, D. Volbers, R. Wyrwich, M. Doblinger, A.S. Susha, A.L. Rogach, F. Jackel, J.K. Stolarczyk, J. Feldmann, Nat. Mater. 13 (2014) 1013–1018.
[43] A.L. Luna, E. Novoseltceva, E. Louarn, P. Beaunier, E. Kowalska, B. Ohtani, M.A. Valenzuela, H. Remita, C. Colbeau-Justin, Appl. Catal. B 191 (2016) 18–28.
[44] Y. Xia, Q. Li, X. Wu, K. Lv, D. Tang, M. Li, Appl. Surf. Sci. 391 (2017) 565–571.
[45] X. Fu, L. Zhang, L. Liu, H. Li, S. Meng, X. Ye, S. Chen, J. Mater. Chem. A 5 (2017) 15287–15293.
[46] W. Feng, Z. Fang, B. Wang, L. Zhang, Y. Zhang, Y. Yang, M. Huang, S. Weng, P. Liu, J. Mater. Chem. A 5 (2017) 1387–1393.
[47] Y. Lv, Y. Liu, Y. Zhu, Y. Zhu, J. Mater. Chem. A 2 (2013) 1174–1182.
[48] Y. Xia, Q. Li, K. Lv, D. Tang, M. Li, Appl. Catal. B 206 (2017) 344–352.
[49] Y. Ye, Z. Zang, T. Zhou, F. Dong, S. Lu, X. Tang, W. Wei, Y. Zhang, J. Catal. 357 (2018) 100–107.
[50] Q. Li, T. Shi, X. Li, K. Lv, M. Li, F. Liu, H. Li, M. Lei, Appl. Catal. B 229 (2018) 8–14.
[51] W. Feng, L. Zhang, Y. Zhang, Y. Yang, Z. Fang, B. Wang, S. Zhang, P. Liu, J. Mater. Chem. A 5 (2017) 10311–10320.
[52] B. Chang, G. Zhao, Y. Shao, L. Zhang, B. Huang, Y. Wu, X. Hao, J. Mater. Chem. A 5 (2017) 18038–18043.
[53] B.E. Conway, B.V. Tilak, Electrochim. Acta 47 (2002) 3571–3594.